

Synthesis, Molecular Characterization, and Antimicrobial Evaluation of Hydrazones Derived from 2-Hydrazinobenzimidazole

Muneera S M Al-Saleem¹, Mohamed S Mohamed Ahmed², Sayed M Riyadh², Awatif H Alruwaili³, Magdi E A Zaki⁴, Sobhi M Gomha⁵

¹Department of Chemistry, College of Science, Princess Nourah Bint Abdulrahman University, P.O. Box 84428, Riyadh, 11671, Saudi Arabia; ²Department of Chemistry, Faculty of Science, Cairo University, Cairo, Egypt; ³Department of Chemistry, College of Science, Northern Border University, Arar, Saudi Arabia; ⁴Department of Chemistry, Faculty of Science, Imam Mohammad Ibn Saud Islamic University (IMSIU), Riyadh, Saudi Arabia; ⁵Department of Chemistry, Faculty of Science, Islamic University of Madinah, Madinah, Saudi Arabia

Correspondence: Sobhi M Gomha; Magdi E A Zaki, Email smgomha@iu.edu.sa; mezaki@imamu.edu.sa

Introduction: Hydrazones, due to the structural diversity of their nitrogen atoms, possess both electrophilic and nucleophilic properties, enabling strong hydrogen bonding interactions with enzymes and receptors. This study aimed to synthesize novel hydrazone derivatives and evaluate their antimicrobial potential.

Methods: Hydrazones were synthesized via condensation of 2-hydrazinobenzimidazole with various aldehydes or ketones using citric acid as an eco-friendly catalyst. The (E)-configuration of the products was confirmed through frontier molecular orbital (FMO) calculations. Antimicrobial activities were assessed against selected Gram-positive and Gram-negative bacteria, and fungi. Molecular docking studies were conducted on the most active compounds (**3c** and **3o**) using bacterial and fungal protein targets (2IWC, 2NXW, 1EA1).

Results: Compounds **3c** and **3o** showed strong antimicrobial activity. Docking studies revealed that both compounds interacted with 2IWC via one H-bond donor to THR531 (3.12 Å), mirroring ampicillin. Against 2NXW, they showed dual H-donor bonding to MET404 with binding energies of -5.96 and -5.72 kcal/mol, comparable to gentamicin. Both also bound ARG326 in 1EA1 with binding energies of -5.97 and -6.0 kcal/mol, similar to nystatin.

Discussion: The comparable binding patterns and energies of compounds **3c** and **3o** to standard antimicrobial agents suggest that they are promising candidates for further development as broad-spectrum antimicrobial agents.

Keywords: condensation, HOMO, LUMO, global descriptors, geometrical configuration, pathogenic microorganisms

Introduction

Green chemistry provides essential principles aimed at minimizing environmental and health hazards by designing safer chemical processes and products. A core goal of this approach is the reduction or elimination of toxic substances through the use of benign solvents, renewable feedstocks, and eco-friendly catalysts.¹ Among these, citric acid has gained considerable attention as a natural, non-toxic, biodegradable, and cost-effective catalyst extracted from citrus fruits (5–7%).² It has been successfully applied in the green synthesis of various heterocyclic compounds, including azoles and azines,² and has facilitated numerous reactions such as Knoevenagel condensation,^{3,4} Schiff bases,^{5–7} imines,⁸ phenolic derivatives,⁹ and amidoalkyl naphthols.¹⁰

In parallel, the pharmaceutical relevance of benzimidazole-based hydrazones has attracted significant research interest due to their broad spectrum of biological activities. These compounds have been reported to possess anti-diabetic,¹¹ anthelmintic,¹² antimicrobial, antioxidant,¹³ anti-inflammatory,¹⁴ anticancer,^{15,16} anticonvulsant,¹⁷ antimalarial,¹⁸ and antileishmanial¹⁹ properties. Furthermore, hydrazones have shown potent inhibitory effects against carbonic anhydrase isoenzymes (I and II),²⁰ making them valuable in rational drug design. Recent advances underscore the therapeutic

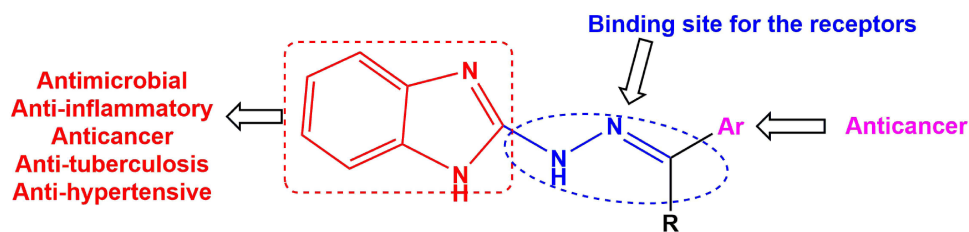


Figure 1 The biological activities of hydrazonebenzimidazole.

potential of benzimidazole derivatives, especially in anticancer and antimicrobial research, with new synthetic strategies enhancing their pharmacological relevance.^{21,22} The hydrazone moiety serves as a versatile pharmacophore capable of binding to various biological receptors,²³ while substitution on the phenyl ring enhances biological activity, including anticancer effects²⁴[Figure 1].

Given the increasing demand for sustainable and biologically active compounds, integrating green chemistry protocols with bioactive scaffold design represents a promising research direction. As part of our ongoing work on green synthesis of heterocycles,^{25–35} we report the citric acid-catalyzed synthesis of benzimidazole-based hydrazones and evaluate their antimicrobial potential. Density Functional Theory (DFT) computations were employed to determine the molecular geometries and electronic properties of the synthesized compounds. Furthermore, molecular docking studies were conducted to gain insights into their interaction with microbial protein targets, supporting their observed biological activities.

Results and Discussion

Chemistry

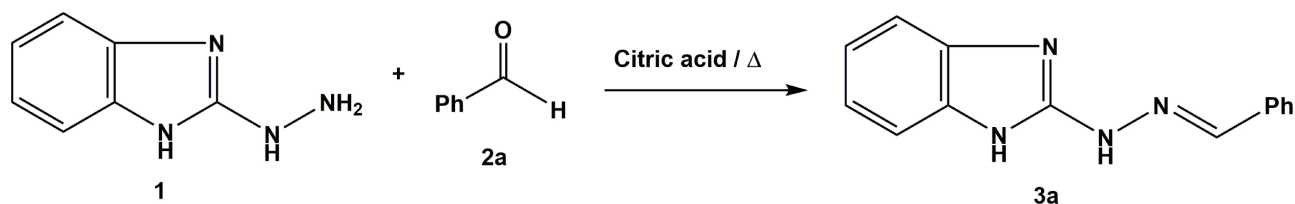
The synthetic conditions for preparing hydrazonebenzimidazole were accomplished by acid catalyst, especially acetic acid in methanol.^{26,35} Our study was commenced on a representative reaction of 2-hydrazinobenzimidazole^{26,35} and benzaldehyde in the presence of (0.1 g) citric acid as an eco-friendly catalyst. The reaction was subjected in various solvents under reflux as shown in Scheme 1 and Table 1.

As illustrated in Table 1, ethanol was a superior solvent in terms of the isolated yield of product 3a.

Ethanol was selected due to its moderate polarity and protic nature, which supports effective solvation of both the hydrazinobenzimidazole and carbonyl substrates. Its hydrogen-bonding ability enhances interactions with the citric acid catalyst, improving proton transfer and reaction kinetics. Additionally, ethanol ensures better miscibility of the reactants and facilitates uniform heat distribution during reflux, contributing to higher product yields.

To generalize the scope of our green synthesis protocol, a series of aromatic aldehydes (**2a–g**) and ketones (**2h–j**), acetyl heterocycles (**2k–n**), and isatin (**2o**) were condensed with 2-hydrazinobenzimidazole (**1**) in ethanol in the presence of acetic acid or citric acid. The mechanistic pathway was illustrated in Scheme 2 and a comparative yield of the condensation products (**3a–o**) was depicted in Table 2.

With the optimal conditions, the condensation reactions have been achieved with citric acid catalyst in good to excellent yield (88–94%) relative to acetic acid (78–85%). 4-substituted benzaldehyde with electron-donating or withdrawing groups gave the respective hydrazones (**3a–3e**) in an excellent yield. Also, dichlorobenzaldehyde with steric



Scheme 1 Reaction of 2-hydrazinobenzimidazole and benzaldehyde.

Table 1 Effect of Solvents on the Product Yield of Compound **3a**

Entry	Solvent	Time (h)	Isolated Yield (%)
1	Methanol	3	85
2	Ethanol	3	94
3	DMF	3	84
4	Dioxane	3	82
5	DMSO	3	80

hinderance was not affected on the yield percent of the products (**3f**, **3g**). Additionally, the high performance of citric acid catalyst was perceived with aryl (**3h-3j**), acetyl heterocycles (**3k-3n**), and isatin (**3o**) as shown in Table 2.

Although hydrazone formation can proceed without a catalyst, the use of citric acid notably enhances reaction efficiency by increasing yields and reducing reaction times. Its role as a natural, biodegradable, and non-toxic acid aligns with green chemistry principles, offering a sustainable alternative to conventional catalysts. This justifies its necessity in promoting an eco-friendly and efficient synthetic protocol.

The theoretical study using Density Functional Theory (DFT) further supports the experimental results. The FMO analysis showed that the (E)-isomers were more stable than the (Z)-isomers in all phases, as indicated by their lower total electronic energies. Moreover, the HOMO-LUMO energy gaps, ionization potentials, and electrophilicity indices provided insights into the reactivity and stability of the compounds. For instance, smaller HOMO-LUMO gaps indicate higher chemical reactivity, which aligns with the biological activity observed in certain hydrazones. Global descriptors such as softness, hardness, and chemical potential also supported the prediction of the compounds' behavior during biological interactions. These findings confirm the reliability of the computational models and their relevance in predicting molecular behavior consistent with antimicrobial activity.

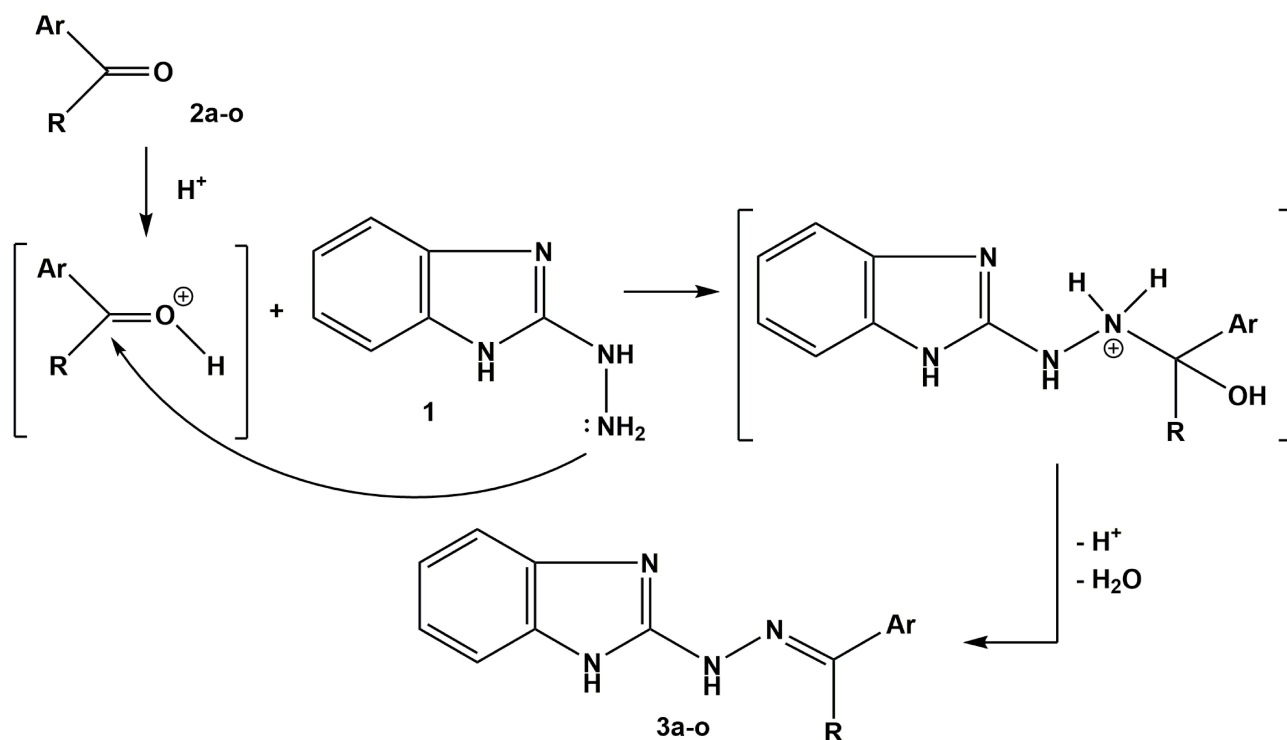
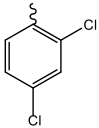
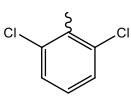
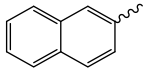
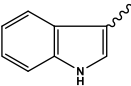
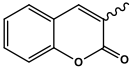
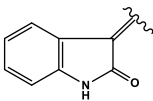
**Scheme 2** Synthesis of hydrazonebenzimidazole (**3a-o**).

Table 2 A Comparative Yield of Products (**3a-o**) Under Catalytic Effect (Acetic Acid and Citric Acid)

Compd. No.	R	Ar	Yield %		Ref.
			Citric Acid	Acetic Acid	
3a	H	C ₆ H ₅	94	85	30
3b	H	4-CH ₃ C ₆ H ₄	92	83	30
3c	H	4-CH ₃ OC ₆ H ₄	92	82	30
3d	H	4-ClC ₆ H ₄	90	83	30
3e	H	4-NO ₂ C ₆ H ₄	90	81	30
3f	H		90	82	-
3g	H		90	80	-
3h	CH ₃	C ₆ H ₅	92	81	31
3i	CH ₃	4-BrC ₆ H ₄	90	80	31
3j	CH ₃		88	78	-
3k	CH ₃		88	79	-
3L	CH ₃		88	80	-
3m	CH ₃		88	81	-
3n	CH ₃		88	82	-

(Continued)

Table 2 (Continued).

Compd. No.	R	Ar	Yield %		Ref.
			Citric Acid	Acetic Acid	
3o			88	80	32

Computational Investigations

The optimized structures of compounds **3a-o** have been generated and displayed in Gauss View 6.0.16 using DFT with the B3LYP function and 6-31G basis set computations using the Gaussian 09 program. The compounds **3a-o** can be formulated in two possible geometrical isomers (*Z*) and (*E*) forms (see Figure 2). HOMO (Highest Occupied Molecular Orbital) and LUMO (Lowest Unoccupied Molecular Orbital) of the investigated compounds in the gas, aqueous, and ethanol phases were computed and summarized in Tables 3, S1, and S2.

The data in Table 3 supported the superiority of the *E*-form over *Z*-form. For example, the electronic energy of **3a** (*E*) in the gas phase = (−476,738.21 Kcal/mol), which is lower than that of **3a** (*Z*) (−476,734.79 Kcal/mol). Similar calculations have been observed in both ethanolic (−476,745.89/−476,741.66 Kcal/mol) and aqueous phases (−476,746.29/−476,742.01 Kcal/mol), respectively.

Additionally, global descriptors such as ionization energy (I), electron affinity (A), global hardness (η), global softness (S), chemical potential (μ), electrophilicity (ω), and nucleophilicity (N) of the synthesized compounds were calculated in three different phases (gas/aqueous/ethanol) as shown in Table 4.

It is worthily mentioned that compounds **3a-o** can be represented in three different tautomeric structures as hydrazones (I), conjugated diazines (II) and benzylazo forms (III) as shown in Figure 3. Frontier Molecular Orbitals (FMO) computations of these tautomeric forms were illustrated in Table 5.

The data in Table 5 pointed out that the electronic energies of tautomeric forms (I, II, and III) of compound **3a** in the gas phase were (−476,738.21, −476,737.53, and −476,723.28 Kcal/mol), respectively, that revealing the superior stability of hydrazone tautomer (I) over conjugated azine tautomer (II) ($\Delta E = 0.68$ Kcal/mol) and benzylazo tautomer (III) ($\Delta E = 14.93$ Kcal/mol). Similarly, the electronic energies of compound **3h** (I, II, and III) in the gas phase were (−501,410.62, −501,410.88, −501,398.75 Kcal/mol), respectively. In the same manner, the electronic energy of (I) is lower than those of (II) and (III) forms in both aqueous and ethanolic phases for compounds **3a** and **3h** (Table 5).

To confirm the stability of hydrazone form (I), the global descriptors of three tautomeric forms (I, II, and III) of compounds **3a** and **3h** were computed in three different phases (gas, aqueous and ethanolic) as summarized in Table S3.

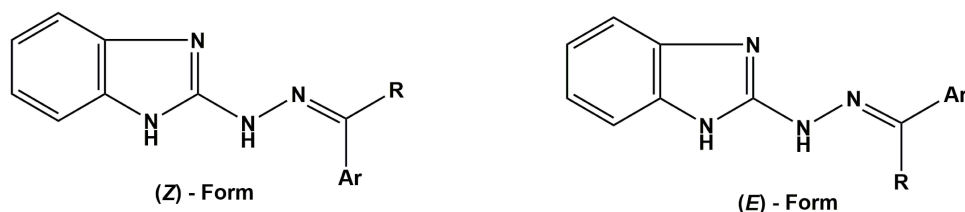
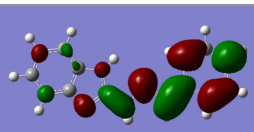
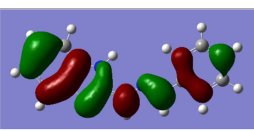
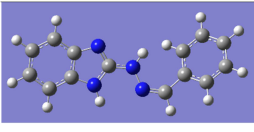
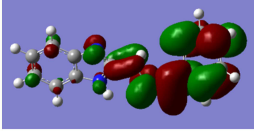
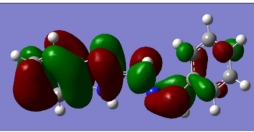
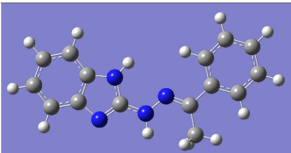
Figure 2 Geometrical isomers of compounds **3a-o**.

Table 3 Frontier Molecular Orbitals (FMO) Computations of Compounds **3a** and **3h**

Compd. No.	Optimized Structure	E (Kcal/mol)		
		Gas	H ₂ O	EtOH
3a (E)		– 476,738.21	– 476,746.29	– 476,745.89
LUMO		E _{LUMO} (eV)		
		Gas	H ₂ O	EtOH
		– 1.46	– 1.42	– 1.42
HOMO		E _{HOMO} (eV)		
		Gas	H ₂ O	EtOH
		– 5.19	– 5.32	– 5.32
3a (Z)		– 476,734.79	– 476,742.01	– 476,741.66
LUMO		E _{LUMO} (eV)		
		Gas	H ₂ O	EtOH
		– 1.42	– 1.37	– 1.37
HOMO		E _{HOMO} (eV)		
		Gas	H ₂ O	EtOH
		– 5.24	– 5.45	– 5.44
3h (E)		– 501,410.62	– 501,419.09	– 501,418.70

(Continued)

Table 3 (Continued).

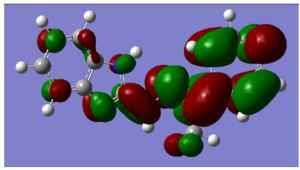
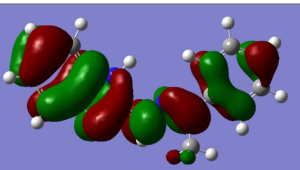
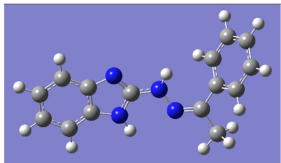
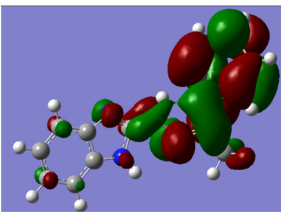
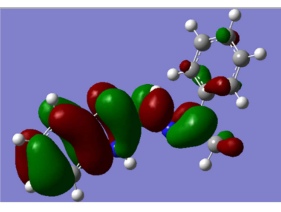
Compd. No.	Optimized Structure	E (Kcal/mol)		
		Gas	H ₂ O	EtOH
LUMO		E _{LUMO} (eV)		
		Gas	H ₂ O	EtOH
		- 1.32	- 1.23	- 1.22
HOMO		E _{HOMO} (eV)		
		Gas	H ₂ O	EtOH
		- 5.14	- 5.31	- 5.30
3h (Z)		E (Kcal/mol)		
		Gas	H ₂ O	EtOH
		- 501,409.57	- 501,417.02	- 501,416.67
LUMO		E _{LUMO} (eV)		
		Gas	H ₂ O	EtOH
		- 1.08	- 0.98	- 0.98
HOMO		E _{HOMO} (eV)		
		Gas	H ₂ O	EtOH
		- 5.09	- 5.35	- 5.34

Table 4 Global Descriptors of Compounds 3a and 3h

No.	I = -E _{HOMO}	A = - E _{LUMO}	$\eta = (E_L - E_H)/2$	S = 1/ η	$\mu = -(I+A)/2$	$\omega = \mu^2/2\eta$	N = E _{HOMO} -E _{HOMO} TCE
3a (E)	5.19	1.46	1.87	0.54	3.33	2.96	4.22
3a (E) /H ₂ O	5.32	1.42	1.95	0.51	3.37	2.91	4.09

(Continued)

Table 4 (Continued).

No.	$I = -E_{\text{HOMO}}$	$A = -E_{\text{LUMO}}$	$\eta = (E_L - E_H)/2$	$S = 1/\eta$	$\mu = -(I+A)/2$	$\omega = \mu^2/2\eta$	$N = E_{\text{HOMO}} - E_{\text{HOMO TCE}}$
3a (E) /EtOH	5.32	1.42	1.95	0.51	3.37	2.91	4.09
3a (Z)	5.24	1.42	1.91	0.52	3.33	2.90	4.17
3a (Z) /H ₂ O	5.45	1.37	2.04	0.49	3.41	2.85	3.96
3a (Z) /EtOH	5.44	1.37	2.04	0.49	3.41	2.85	3.97
3h (E)	5.14	1.32	1.91	0.52	3.23	2.73	4.27
3h (E) /H ₂ O	5.31	1.23	2.04	0.49	3.27	2.62	4.10
3h (E) /EtOH	5.30	1.22	2.04	0.49	3.26	2.60	4.11
3h (Z)	5.09	1.08	2.01	0.50	3.09	2.37	4.32
3h (Z) /H ₂ O	5.35	0.98	2.19	0.46	3.17	2.29	4.06
3h (Z) /EtOH	5.34	0.98	2.18	0.46	3.16	2.29	4.07

The in vitro Antimicrobial Screening

The synthesized compounds **3a-o** were evaluated in vitro for their antimicrobial activity against two Gram-positive bacteria: *Bacillus subtilis* (BS, ATCC 6633) and *Staphylococcus aureus* (SA, ATCC 6538), and two Gram-negative bacteria: *Pseudomonas aeruginosa* (PA, ATCC 90274) and *Klebsiella pneumoniae* (KP, ATCC 13883). Additionally, one yeast, *Candida albicans* (CA, ATCC 10221), and one fungus, *Aspergillus fumigatus* (AF, ATCC 14109), were also tested. The standard drugs used for comparison were Gentamicin (Gram-positive bacteria), Ampicillin (Gram-negative bacteria) and Nystatin (fungi). The antimicrobial activity was assessed by measuring the inhibition zone diameter (IZD) in mm/mg of sample at a concentration of 30 $\mu\text{g/mL}$ for each compound. The results were summarized in Table 6.

The results presented in Table 6 revealed varying levels of antimicrobial efficacy across the tested microorganisms. The synthesized compounds exhibited diverse degrees of activity against Gram-positive and Gram-negative bacteria. Among the tested compounds, **3c** displayed exceptional activity against Gram-positive bacteria, with inhibition zone

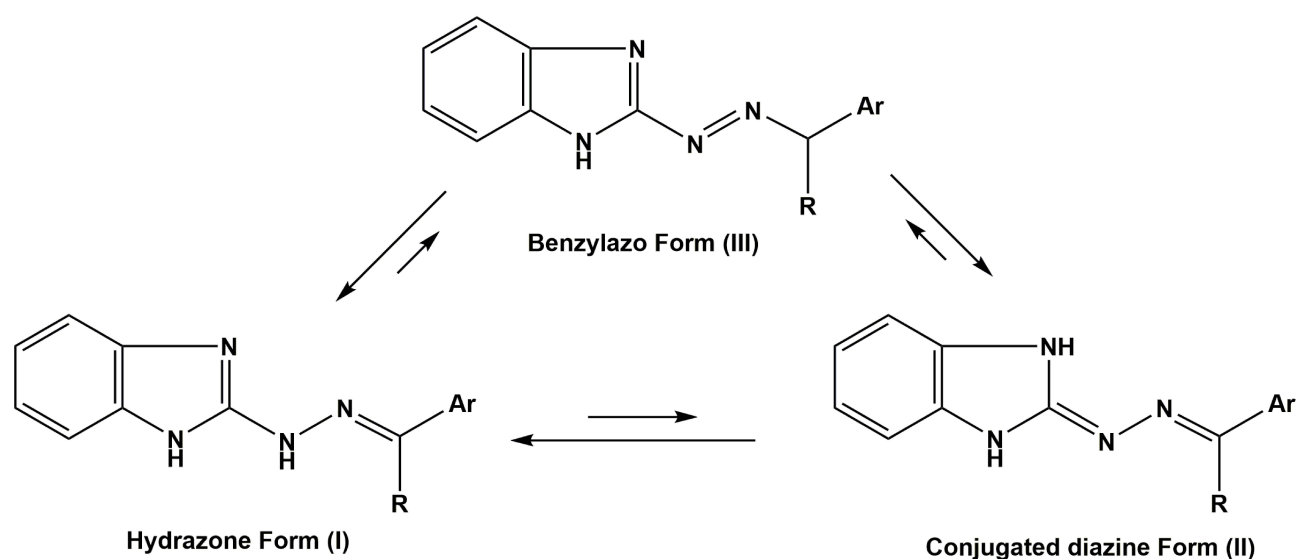
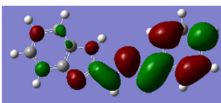
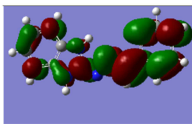
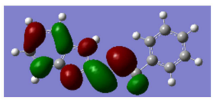
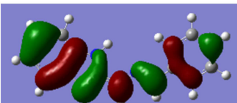
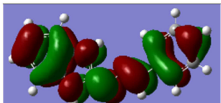
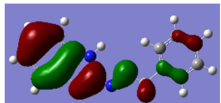


Figure 3 Tautomeric forms of compounds **3a-o**.

Table 5 (FMO) Computations of the Tautomeric Forms (I, II, and III) of **3a** and **3h**

Compd. (3a)		E (I)	E (II)	E (III)
Optimized structure				
E (Kcal/mol)	Gas	- 476,738.21	- 476,737.53	- 476,723.28
	H ₂ O	- 476,746.29	- 476,745.10	- 476,730.62
	EtOH	- 476,745.89	- 476,744.72	- 476,730.24
LUMO				
E _{LUMO} (eV)	Gas	- 1.46	- 1.01	- 2.35
	H ₂ O	- 1.42	- 1.23	- 2.45
	EtOH	- 1.42	- 1.22	- 2.45
HOMO				
E _{HOMO} (eV)	Gas	- 5.19	- 4.88	- 6.24
	H ₂ O	- 5.32	- 5.03	- 6.34
	EtOH	- 5.32	- 5.03	- 6.34
Compd. (3h)		E (I)	E (II)	E (III)
Optimized structure				
E (Kcal/mol)	Gas	- 501,410.62	- 501,410.88	- 501,398.75
	H ₂ O	- 501,419.09	- 501,418.06	- 501,406.05
	EtOH	- 501,418.70	- 501,417.69	- 501,404.54

(Continued)

Table 5 (Continued).

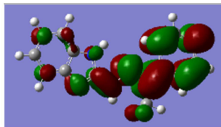
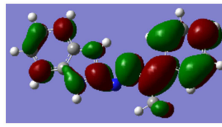
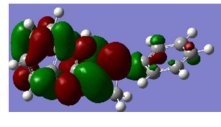
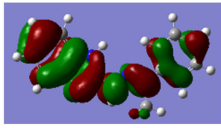
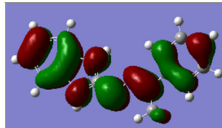
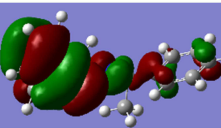
LUMO				
E_{LUMO} (eV)	Gas	- 1.32	- 0.89	- 2.15
	H ₂ O	- 1.23	- 1.09	- 2.32
	EtOH	- 1.22	- 1.08	- 2.26
HOMO				
E_{HOMO} (eV)	Gas	- 5.14	- 4.84	- 6.18
	H ₂ O	- 5.31	- 4.98	- 6.35
	EtOH	- 5.30	- 4.97	- 6.31

Table 6 Preliminary Antimicrobial Activity for the Synthesized Compounds 3a-o

Compd.	Pathogenic Microorganisms mm					
	Gram Positive Bacteria		Gram Negative Bacteria		Yeast	Fungi
	<i>Bacillus subtilis</i>	<i>Staphylococcus aureus</i>	<i>Pseudomonas aeruginosa</i>	<i>Klebsiella pneumoniae</i>	<i>Candida albicans</i>	<i>Aspergillus fumigatus</i>
3a	26.5 ± 0.9	25.3 ± 0.8	20.1 ± 0.8	NA	22.4 ± 0.8	NA
3b	27.0 ± 0.8	28.2 ± 0.6	22.8 ± 0.9	29.8 ± 0.9	27.7 ± 0.7	NA
3c	29.2 ± 0.7	31.7 ± 0.9	26.3 ± 0.7	32.2 ± 1.0	29.8 ± 0.7	21.3 ± 0.5
3d	25.2 ± 0.8	27.1 ± 0.8	18.4 ± 0.7	23.3 ± 0.7	22.3 ± 0.7	NA
3e	NA	22.3 ± 0.9	NA	21.9 ± 0.8	23.2 ± 0.8	NA
3f	NA	20.5 ± 0.8	NA	NA	24.8 ± 0.9	NA
3g	23.4 ± 0.9	19.7 ± 0.5	21.0 ± 0.7	NA	27.6 ± 0.7	NA
3h	29.0 ± 1.0	29.4 ± 0.9	25.6 ± 0.5	29.2 ± 0.8	27.5 ± 0.9	15.6 ± 0.8
3i	23.2 ± 0.9	26.1 ± 0.9	21.0 ± 0.8	NA	24.6 ± 0.8	NA
3j	27.6 ± 0.9	29.4 ± 0.7	21.2 ± 0.9	29.8 ± 0.7	20.9 ± 0.8	19.4 ± 0.7
3k	29.6 ± 0.7	30.9 ± 0.9	21.8 ± 0.7	28.5 ± 0.8	28.4 ± 0.9	17.7 ± 0.8
3L	28.3 ± 1.3	29.7 ± 0.9	21.9 ± 0.6	27.8 ± 1.1	26.6 ± 0.8	18.6 ± 0.9

(Continued)

Table 6 (Continued).

Compd.	Pathogenic Microorganisms mm					
	Gram Positive Bacteria		Gram Negative Bacteria		Yeast	Fungi
	<i>Bacillus subtilis</i>	<i>Staphylococcus aureus</i>	<i>Pseudomonas aeruginosa</i>	<i>Klebsiella pneumoniae</i>	<i>Candida albicans</i>	<i>Aspergillus fumigatus</i>
3m	29.0 ± 0.8	30.0 ± 0.9	21.9 ± 0.6	27.6 ± 0.8	25.0 ± 0.7	20.5 ± 0.7
3n	28.3 ± 0.8	31.0 ± 0.8	22.7 ± 0.8	27.8 ± 0.6	25.3 ± 0.7	21.7 ± 0.8
3o	29.6 ± 0.7	31.9 ± 0.7	23.7 ± 0.6	28.5 ± 0.9	25.9 ± 0.6	25.0 ± 0.9
Ampicillin	29.7 ± 0.9	30.2 ± 0.8	–	–	–	–
Gentamicin	–	–	29.8 ± 0.8	28.3 ± 0.5	–	–
Nystatin	–	–	–	–	29.4 ± 0.8	33.4 ± 0.9

Notes: Values are mean inhibition zone diameter (mm) ± standard deviation of three replicates. Mean zone of inhibition measured in millimeters, generated by several pathogenic bacteria. Control for Bacteria was Gentamycin and for fungi was Fluconazole.

Abbreviation: NA, No activity.

diameters (IZDs) of 31.7 ± 0.9 mm against *S. aureus* and 29.2 ± 0.7 mm against *B. subtilis*, closely approximating the activity of the standard ampicillin (30.2 ± 0.8 mm and 29.7 ± 0.9 mm, respectively). Similarly, compounds **3h**, **3j**, **3k**, **3L**, **3m**, **3n**, and **3o** demonstrated strong activity against both Gram-positive strains, with IZDs ranging from 27.6 to 31.9 mm.

Against Gram-negative bacteria, **3c** exhibited superior activity, particularly against *K. pneumoniae*, with an IZD of 32.2 ± 1.0 mm, surpassing the efficacy of Gentamicin (28.3 ± 0.5 mm). Other compounds, including **3b**, **3h**, and **3j–3o**, also displayed considerable activity against *K. pneumoniae*, with IZDs between 27.6 and 29.8 mm. Notably, **3c** and **3h** demonstrated significant activity against *P. aeruginosa*, with IZDs of 26.3 ± 0.7 mm and 25.6 ± 0.5 mm, respectively. These results underscore the potential of these compounds as effective agents against Gram-negative bacterial infections.

The antifungal activity of the compounds was evaluated against *C. albicans* and *A. fumigatus*. Most compounds showed promising activity against *C. albicans*, with **3c** exhibiting the highest activity (IZD: 29.8 ± 0.7 mm), surpassing the standard nystatin (29.4 ± 0.8 mm). Compounds **3b**, **3h**, **3k**, and **3L** also demonstrated strong activity against *C. albicans*, with IZDs ranging from 26.6 to 28.4 mm. For *A. fumigatus*, moderate activity was observed. Compound **3o** exhibited the highest activity, with an IZD of 25.0 ± 0.9 mm, although it was less effective than nystatin (33.4 ± 0.9 mm). Compounds **3c**, **3h**, **3j**, **3k**, **3L**, **3m**, and **3n** demonstrated moderate activity against *A. fumigatus*, with IZDs ranging from 15.6 to 21.7 mm.

Structure-Activity Relationship (SAR) of Synthesized Hydrazones (3a–o)

The antimicrobial activity of the synthesized hydrazones (**3a–o**) is strongly influenced by specific structural modifications. Electron-donating groups, such as $-\text{OCH}_3$ (in **3c**) and $-\text{CH}_3$ (in **3b**), significantly enhanced antimicrobial potency compared to electron-withdrawing substituents. This improvement likely stems from increased electron density on the aromatic ring, which facilitates stronger hydrogen bonding and π – π interactions with microbial targets. Conversely, compounds with strong electron-withdrawing groups exhibited reduced activity, underscoring the advantage of electron-rich systems in promoting target engagement.

Heteroaromatic substitutions further boosted efficacy, with derivatives containing thiophene, pyridine, indole, or coumarin (**3k–3n**) showing markedly improved activity. The planarity and heteroatom interactions of these moieties are proposed to enhance both target affinity and membrane permeability. Lipophilicity also played a critical role: bulkier, more lipophilic compounds (eg, **3j** with naphthyl and **3o** with isatin) demonstrated superior activity, likely due to improved penetration of microbial lipid bilayers, as supported by their stronger docking scores. Notably, steric hindrance was well-tolerated, as evidenced by the retained activity of dichloro-substituted derivatives (**3f**, **3g**), suggesting flexibility for further structural optimization.

The most potent compounds (**3c** and **3o**) exhibited a consistent correlation between their electronic properties, binding interactions, and biological activity. Their small HOMO-LUMO gaps (indicating favorable charge transfer) and strong hydrogen-bonding interactions with key microbial residues align with their exceptional in vitro performance. Collectively, these findings highlight that antimicrobial potency in hydrazones can be maximized by incorporating electron-donating groups, heterocyclic rings, and lipophilic features—strategies that synergistically improve target binding, membrane penetration, and overall bioavailability.

Molecular Docking

The molecular docking evaluation was performed using the Molecular Operating Environment (MOE) software. The interaction between the selected proteins (PDB: 2IWC, 2NXW, and 1EA1) is utilized to assess the antimicrobial activity of the most promising hydrazone derivatives (**3c** and **3o**) using Ampicillin, Gentamicin, and Nystatin as benchmark antibiotics (essential antimicrobial references). A comparison study between the ligands and antimicrobial references depended on the number of hydrogen bond interactions, the binding energy score, and the distance apart between the ligand/reference antibiotic and crucial amino acid residues in the protein. The investigation results for the interaction between antimicrobial references (Ampicillin/Gentamicin/Nystatin) or ligands (**3c** and **3o**) with different proteins (2IWC as a gram-positive bacterial strain, 2NXW as a gram-negative bacterial strain and 1EA1 as antifungal strain) were shown in Table 7.

Ampicillin had a binding energy score = -6.07 Kcal/mol (RMSD = 1.39) with 2IWC protein (Table 7). It exhibited five H-bond interactions (one H-donor and four H-acceptors). The H-acceptor interactions with THR531, ASN441,

Table 7 Ligand-Protein Interaction of the Antibiotics and Compounds (**3c**, **3o**) with Proteins

Compd.	Protein	Ligand-Protein Interactions/Type of Interactions	Binding Energy (Kcal/mol)	Root Mean Square Deviation RMSD	Bond Distance (Å)
Ampicillin	2IWC	THR 531 (A) / H-donor THR 531 (A) / H-acceptor ASN 441 (A) / H-acceptor ILE 533 (A) / H-acceptor SER 439 (A) / H-acceptor ASN 478 (A) / pi-H	- 6.07	1.39	3.30 2.98 3.04 3.16 3.40 3.6
3c	2IWC	THR 531 (A) H-donor ASN 441 (A) H-donor ASN 441 (A) H-acceptor ILE 533 (A) pi-H	- 5.63	1.09	2.99 3.35 3.13 4.03
3o	2IWC	THR 531 (A) H-donor GLY 530 (A) H-acceptor TYR 438 (A) pi-H ASN 441 (A) pi-H	- 5.24	1.93	2.94 3.34 3.77 3.85
Gentamicin	2NXW	MET 434 (A) / H-donor MET 404 (A) / H-donor MET 404 (A) / H-donor ALA 402 (A) / H-donor	- 5.18	1.55	4.41 3.96 4.17 2.94
3c	2NXW	MET 404 (A) / H-donor MET 404 (A) / H-donor TRP 459 (A) / pi-H	- 5.96	1.21	3.24 3.53 4.81
3o	2NXW	MET 404 (A) H-donor LEU 462 (A) H-acceptor TRP 459 (A) pi-pi	- 5.26	0.98	3.46 3.32 3.92

(Continued)

Table 7 (Continued).

Compd.	Protein	Ligand-Protein Interactions/Type of Interactions	Binding Energy (Kcal/mol)	Root Mean Square Deviation RMSD	Bond Distance (Å)
Nystatin	IEAI	HIS 392 (A) / H-donor	- 4.32	2.4	2.51
		SER 261 (A) / H-donor			2.55
		PRO 386 (A) / H-donor			2.72
		TYR 76 (A) / H-acceptor			2.72
		ARG 326 (A) / H-acceptor			2.79
3c	IEAI	ARG 326 (A) H-acceptor	- 6.16	1.21	2.87
		ALA 256 (A) pi-H			4.38
3o	IEAI	ARG 326 (A) H-acceptor	- 5.75	0.95	3.44
		ARG 95 (A) pi-cation			4.65
		ARG 95 (A) pi-cation			4.14
		ARG 96 (A) pi-cation			3.99
		ARG 96 (A) pi-cation			3.17

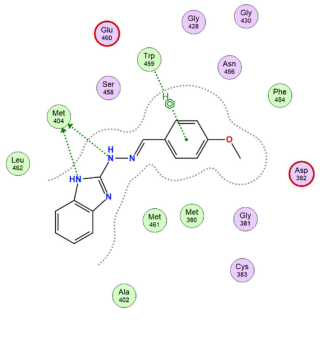
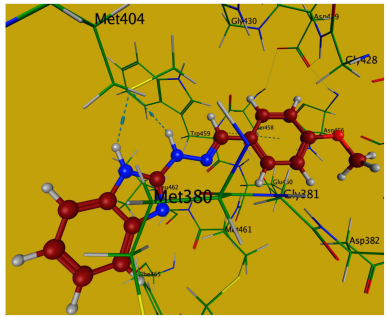
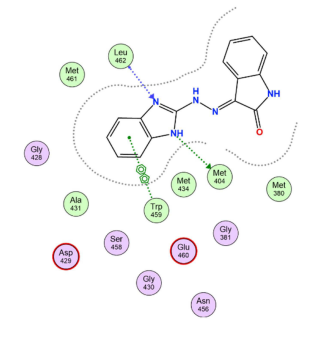
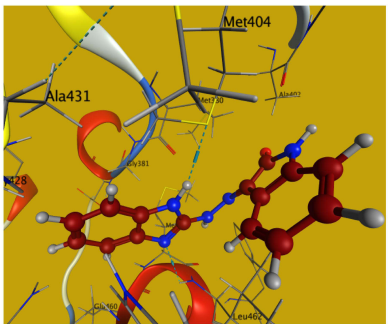
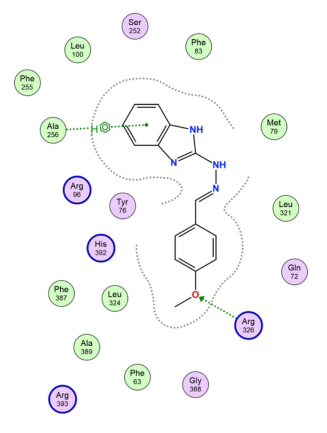
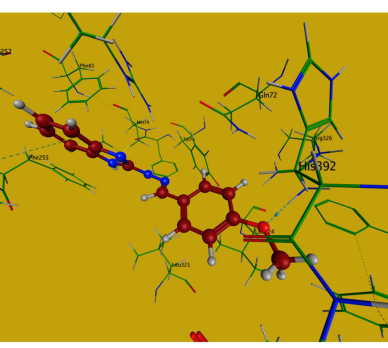
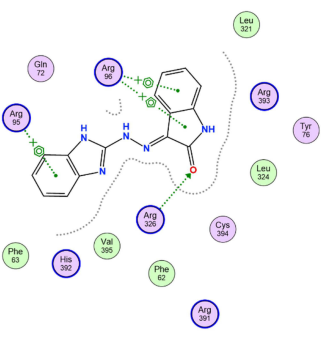
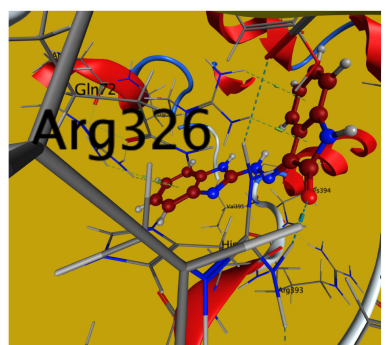
ILE533, and SER439 with 2.98, 3.04, 3.16, and 3.40 Å, respectively, in addition to an H-donor bond with THR531 with 3.32 Å. Compounds **3c** and **3o** interacted with 2IWC through binding energy scores of -5.63 and -5.24 Kcal/mol, respectively. **3c** as a model example displayed three H-bonds (two H-bond donors with side chain amino acid THR531 and main chain amino acid ASN441) and one H-bond acceptor main chain amino acid ASN441. The investigated candidates bounded to the same amino acid (S) as the reference antibiotic ampicillin. Thus, the inhibition efficacy of the tested compounds against gram-positive bacteria is confirmed by these interactions (Tables 7 and 8).

Table 8 2D and 3D of Ligand's Interaction (3c and 3o) with 2IWC, 2NXW, and IEAI Proteins

No.	Protein	2D	3D
3c	2IWC		
3o	2IWC		

(Continued)

Table 8 (Continued).

No.	Protein	2D	3D
3c	2NXW		
3o	2NXW		
3c	IEA1		
3o	IEA1		

Similarly, the interaction of gentamicin with 2NXW protein (Table 7) was substantiated via four H-donor bonds with amino acids MET404, MET434, and ALA402, with binding energy (-5.18 Kcal/mol) and RMSD = 1.55 Å. Compounds **3c** as a model example bonded with 2NXW protein via two H-donor bonds with the main chain amino acid MET404 and one pi-H bond with the main chain amino acid TRP459, that reflected the inhibition potency of these compounds towards gram-negative bacterial strain (Tables 8). Additionally, binding of nystatin with 1EA1, as a fungal protein, was achieved (Table 7) via three H-donor bonds with the amino acids HIS392, SER261, and PRO386, and two H-acceptor bonds with TYR76 and ARG326 amino acids with binding energies = -4.32 Kcal/mol. Both compounds **3c** and **3o** were consistently connected to the same amino acid residue (ARG326) in 1EA1 protein with binding energies of -6.16 and -5.75 Kcal/mol, respectively, that supported the biological activity of the tested compounds (**3c** and **3o**) against *C. albicans* and *A. fumigatus* (Tables 7 and 8).

The 2D and 3D images of the ligand's interaction (**3c** and **3o**) with 2IWC, 2NXW, and 1EA1 proteins were compiled in Table 8.

Experimental

Materials and Instruments

A digital melting point apparatus (Bibby Sci. Lim. Stone, Staffordshire, UK) was used to measure the melting points (uncorrected) of products **3a-o**. Shimadzu FTIR 8101 PC infrared spectrophotometer (Shimadzu, Tokyo, Japan) has recorded IR spectra in potassium bromide discs. Recording of $^1\text{H-NMR}$ (at 300 MHz) and $^{13}\text{C-NMR}$ (at 75 MHz) spectra was manipulated on A Varian Mercury VXR-300 spectrometer using tetramethyl silane as an internal standard. The samples were dissolved in deuterated dimethylsulfoxide (DMSO- d_6). GCMS-Q1000-EX Shimadzu spectrometer measured Mass spectra at an ionizing voltage of 70 eV. A German-made Elementarvario LIII CHNS analyzer was used to measure the elemental analyses of the synthesized products.

General Procedure for the Reactions of 2-Hydrazonebenzimidazole (1) and Carbonyl Compounds

A mixture of 2-hydrazonebenzimidazole (**1**) [0.148 g, 1 mmol] and carbonyl compounds **2a-o** (1 mmol of each) in ethanol (20 mL) and few drops of acetic acid (or 0.1 g citric acid) was refluxed for 3 hours (checked by TLC until complete disappearance of starting materials). After evaporation of excess ethanol under reduced pressure, the collected precipitate was filtered and recrystallized from the appropriate solvent to give pure products **3a-o**.

2-(2-Benzylidenehydrazinyl)-1H-Benzo[d]imidazole (3a)

Yellow powder, mp = 293 – 295°C , [lit. mp = 291°C]³⁶ (EtOH/DMF); IR (KBr) ν = 3432 (NH), 2923 (CH-), 1600 (C=N) cm^{-1} ; $^1\text{H-NMR}$ (DMSO- d_6) δ : 7.09–7.51 (m, 9H, Ar-H), 8.33 (s, 1H, CH=N), 10.72 (s, 1H, NH), 12.53 (s, 1H, NH) ppm; $^{13}\text{C-NMR}$ (DMSO- d_6): δ : 113.1, 114.4, 122.5, 123.9, 126.2, 127.8, 137.1, 141.5, 143.0, 149.7, 150.1, 158.1 (Ar-C) ppm; MS, m/z (%) 236 (M^+ , 31), 197 (61), 155 (54), 116 (100), 89 (32). Anal. Calcd. For $\text{C}_{14}\text{H}_{12}\text{N}_4$ (236.11): C, 71.17; H, 5.12; N, 23.71. Found: C, 71.29; H, 5.28; N, 23.91%.

2-[2-(4-Methylbenzylidene)hydrazinyl]-1H-Benzo[d]imidazole (3b)³⁶

Yellow powder, mp = 275 – 277°C , [lit. mp = 277°C] (DMF); IR (KBr) ν = 3430 (NH), 2919 (CH-), 1602 (C=N) cm^{-1} ; $^1\text{H-NMR}$ (DMSO- d_6) δ : 2.38 (s, 3H, CH_3), 7.10–7.52 (m, 8H, Ar-H), 8.31 (s, 1H, CH=N), 10.74 (s, 1H, NH), 12.53 (s, 1H, NH) ppm; $^{13}\text{C-NMR}$ (DMSO- d_6): δ : 20.4 (CH_3), 114.4, 115.1, 122.3, 123.4, 126.9, 128.8, 131.4, 132.4, 136.2, 140.8, 144.4, 150.8 (Ar-C) ppm; MS, m/z (%) 250 (M^+ , 43), 136 (57), 121 (100), 95 (25). Anal. Calcd. For $\text{C}_{15}\text{H}_{14}\text{N}_4$ (250.12): C, 71.98; H, 5.64; N, 22.38. Found: C, 72.09; H, 5.73; N, 22.21%.

2-[2-(4-Methoxybenzylidene)hydrazinyl]-1H-Benzo[D]imidazole (3c)³⁶

Yellow powder, mp = 215 – 217°C , [lit. mp = 212°C] (EtOH); IR (KBr) ν = 3412, 3204 (NH), 30212 (CH=), 2960, 2914 (CH-), 1602 (C=N) cm^{-1} ; $^1\text{H-NMR}$ (DMSO- d_6) δ : 3.69 (s, 3H, OCH_3), 7.11–7.56 (m, 8H, Ar-H), 8.33 (s, 1H, CH=N),

10.68 (s, 1H, NH), 12.52 (s, 1H, NH) ppm; $^{13}\text{C-NMR}$ (DMSO- d_6): δ : 56.2 (OCH₃), 114.3, 121.5, 128.4, 128.8, 129.3, 129.6, 129.8, 130.0, 146.4, 148.5, 152.3, 158.0 (Ar-C) ppm; MS, m/z (%) 266 (M⁺, 52), 158 (85), 142 (100), 138 (89), 89 (86), 75 (43). Anal. Calcd. For C₁₅H₁₄N₄O (266.12): C, 67.65; H, 5.30; N, 21.04. Found: C, 67.49; H, 5.18; N, 20.91%.

2-[2-(4-Chlorobenzylidene)hydrazinyl]-1H-Benzo[D]imidazole (3d)³⁶

Yellow powder, mp = 273–275°C, [lit. mp = 270°C] (DMF); IR (KBr) ν = 3426, 3246 (NH), 3024 (CH=), 2959 (CH-), 1596 (C=N) cm⁻¹; $^1\text{H NMR}$ (DMSO- d_6): δ : 7.18–7.92 (m, 8H, Ar-H), 8.72 (s, 1H, CH=N), 10.70 (s, 1H, NH), 12.51 (s, 1H, NH) ppm; $^{13}\text{C-NMR}$ (DMSO- d_6): δ : 115.1, 115.8, 122.3, 123.4, 128.9, 129.2, 130.2, 132.4, 135.2, 142.8, 148.4, 160.8 (Ar-C) ppm; MS, m/z (%) 270 (M⁺, 40), 188 (46), 150 (89), 75 (100). Anal. Calcd. For C₁₄H₁₁ClN₄ (270.07): C, 62.11; H, 4.10; N, 20.70. Found: C, 62.19; H, 4.17; N, 20.55%.

2-[2-(4-Nitrobenzylidene)hydrazinyl]-1H-Benzo[D]imidazole (3e)³⁶

Yellow powder, mp = 287–289°C, [lit. mp = 283°C] (DMF); IR (KBr) ν = 3451 (NH), 3013 (CH=), 1594 (C=N) cm⁻¹; $^1\text{H NMR}$ (DMSO- d_6): δ : 7.10–7.89 (m, 8H, Ar-H), 8.62 (s, 1H, CH=N), 10.28 (s, 1H, NH), 12.53 (s, 1H, NH) ppm; $^{13}\text{C-NMR}$ (DMSO- d_6): δ : 115.2, 116.1, 123.4, 124.3, 125.2, 125.9, 132.2, 136.4, 139.2, 142.1, 150.4, 160.8 (Ar-C) ppm; MS, m/z (%) 281 (M⁺, 20), 203 (52), 187 (53), 102 (100), 75 (80). Anal. Calcd. For C₁₄H₁₁N₅O₂ (281.09): C, 59.78; H, 3.94; N, 24.90. Found: C, 59.55; H, 4.07; N, 24.85%.

2-[2-(2,4-Dichlorobenzylidene)hydrazinyl]-1H-Benzo[D]imidazole (3f)

Yellow powder, mp = 247–249°C (EtOH); IR (KBr) ν = 3433, 3203 (NH), 2958, 2918 (CH-), 1598 (C=N) cm⁻¹; $^1\text{H NMR}$ (DMSO- d_6): δ : 7.10–7.89 (m, 7H, Ar-H), 8.72 (s, 1H, CH=N), 10.28 (s, 1H, NH), 12.53 (s, 1H, NH) ppm; $^{13}\text{C-NMR}$ (DMSO- d_6): δ : 114.8, 115.3, 122.4, 123.4, 123.9, 127.5, 128.2, 129.3, 130.2, 131.4, 131.9, 132.8, 138.4, 160.7 (Ar-C) ppm; MS, m/z (%) 304 (M⁺, 31), 279 (36), 231 (49), 154 (56), 127 (100), 77 (39). Anal. Calcd. For C₁₄H₁₀Cl₂N₄ (304.03): C, 55.10; H, 3.30; N, 18.36. Found: C, 55.19; H, 3.19; N, 18.25%.

2-[2-(2,6-Dichlorobenzylidene)hydrazinyl]-1H-Benzo[D]imidazole (3g)

Yellow powder, mp = 271–273°C (DMF); IR (KBr) ν = 3425 (NH), 2915 (CH-), 1603 (C=N) cm⁻¹; $^1\text{H NMR}$ (DMSO- d_6): δ : 7.11–7.89 (m, 7H, Ar-H), 8.72 (s, 1H, CH=N), 10.29 (s, 1H, NH), 12.53 (s, 1H, NH) ppm; $^{13}\text{C-NMR}$ (DMSO- d_6): δ : 114.8, 115.2, 123.4, 123.9, 124.6, 127.5, 128.2, 129.3, 130.2, 131.4, 131.9, 133.8, 138.4, 160.6 (Ar-C) ppm; MS, m/z (%) 304 (M⁺, 62), 251 (60), 194 (36), 173 (100), 133 (63), 73 (92). Anal. Calcd. For C₁₄H₁₀Cl₂N₄ (304.03): C, 55.10; H, 3.30; N, 18.36. Found: C, 55.20; H, 3.19; N, 18.18%.

2-[2-(1-Phenylethylidene)hydrazinyl]-1H-Benzo[D]imidazole (3h)³⁷

Yellow powder, mp = 237–239°C (EtOH); IR (KBr) ν = 3432 (NH), 3035 (CH=), 2912 (CH-), 1599 (C=N) cm⁻¹; $^1\text{H NMR}$ (DMSO- d_6): δ : 2.46 (s, 3H, CH₃), 7.09–7.52 (m, 9H, Ar-H), 10.52 (s, 1H, NH), 12.45 (s, 1H, NH) ppm; $^{13}\text{C-NMR}$ (DMSO- d_6): δ : 18.4 (CH₃), 115.4, 116.1, 123.3, 123.7, 124.9, 128.1, 128.4, 130.4, 135.2, 136.8, 141.4, 160.8 (Ar-C) ppm; MS, m/z (%) 250 (M⁺, 70), 192 (48), 160 (96), 112 (100), 76 (82). Anal. Calcd. For C₁₅H₁₄N₄ (250.12): C, 71.98; H, 5.64; N, 22.38. Found: C, 72.03; H, 5.71; N, 22.28%.

2-[2-(1-(4-Bromophenyl)ethylidene)hydrazinyl]-1H-Benzo[D]imidazole (3i)³⁷

Yellow powder, mp = 250–252°C (EtOH); IR (KBr) ν = 3385 (NH), 1585 (C=N) cm⁻¹; $^1\text{H NMR}$ (DMSO- d_6): δ : 2.47 (s, 3H, CH₃), 7.10–7.74 (m, 8H, Ar-H), 10.54 (s, 1H, NH), 12.49 (s, 1H, NH) ppm; $^{13}\text{C-NMR}$ (DMSO- d_6): δ : 18.6 (CH₃), 115.4, 116.2, 123.3, 123.7, 124.9, 128.1, 128.6, 130.4, 134.9, 136.6, 141.4, 160.7 (Ar-C) ppm; MS, m/z (%) 328 (M⁺, 37), 197 (67), 138 (69), 126 (100), 116 (87), 77 (48). Anal. Calcd. For C₁₅H₁₃BrN₄ (328.03): C, 54.73; H, 3.98; N, 17.02. Found: C, 54.81; H, 3.77; N, 16.88%.

2-[2-(1-(Naphthalen-2-Yl)ethylidene)hydrazinyl]-1H-Benzo[D]imidazole (3j)

Yellow powder, mp = 288–290°C, (DMF); IR (KBr) ν = 3414, 3204 (NH), 2915 (CH-), 1601 (C=N) cm^{-1} ; ^1H NMR (DMSO- d_6) δ : 2.46 (s, 3H, CH₃), 7.11–8.45 (m, 11H, Ar-H), 10.62 (s, 1H, NH), 12.53 (s, 1H, NH) ppm; ^{13}C -NMR (DMSO- d_6): δ : 18.8 (CH₃), 114.9, 115.1, 122.8, 123.1, 126.4, 126.8, 127.2, 127.6, 128.3, 128.6, 129.2, 129.8, 131.9, 133.2, 134.2, 135.8, 142.4, 158.1 (Ar-C) ppm; MS, m/z (%) 300 (M^+ , 100), 247 (19), 219 (15), 140 (33). Anal. Calcd. For C₁₉H₁₆N₄ (300.14): C, 75.98; H, 5.37; N, 18.65. Found: C, 76.09; H, 5.48; N, 18.81%.

2-[2-(1-(Thiophen-2-Yl)ethylidene)hydrazinyl]-1H-Benzo[D]imidazole (3k)

Yellow powder, mp = 244–246°C, (EtOH); IR (KBr) ν = 3433 (NH), 2921 (CH-), 1596 (C=N) cm^{-1} ; ^1H NMR (DMSO- d_6) δ : 2.47 (s, 3H, CH₃), 7.11–7.63 (m, 7H, Ar-H), 10.60 (s, 1H, NH), 12.54 (s, 1H, NH) ppm; ^{13}C -NMR (DMSO- d_6): δ : 18.7 (CH₃), 114.9, 115.2, 123.1, 124.4, 124.8, 125.2, 127.6, 128.1, 134.4, 135.8, 142.4, 158.7 (Ar-C) ppm; MS, m/z (%) 256 (M^+ , 71), 199 (39), 184 (100), 127 (66), 77 (68). Anal. Calcd. For C₁₃H₁₂N₄S (256.08): C, 60.92; H, 4.72; N, 21.86; S, 12.51. Found: C, 61.09; H, 4.68; N, 21.88; S, 12.36%.

2-[2-(1-(Pyridin-3-Yl)ethylidene)hydrazinyl]-1H-Benzo[D]imidazole (3l)

Yellow powder, mp = 263–265°C (EtOH/DMF); IR (KBr) ν = 3387 (NH), 1592 (C=N) cm^{-1} ; ^1H NMR (DMSO- d_6) δ : 2.43 (s, 3H, CH₃), 7.09–8.67 (m, 8H, Ar-H), 10.58 (s, 1H, NH), 12.42 (s, 1H, NH) ppm; ^{13}C -NMR (DMSO- d_6): δ : 19.3 (CH₃), 115.2, 115.9, 122.3, 123.7, 123.9, 126.1, 132.4, 133.2, 134.2, 136.8, 141.4, 145.2, 160.4 (Ar-C) ppm; MS, m/z (%) 251 (M^+ , 65), 204 (45), 123 (44), 106 (98), 91 (100). Anal. Calcd. For C₁₄H₁₃N₅ (251.12): C, 66.92; H, 5.21; N, 27.87. Found: C, 67.03; H, 5.33; N, 27.91%.

2-[2-(1-(1H-Indol-3-Yl)ethylidene)hydrazinyl]-1H-Benzo[D]imidazole (3m)

Yellow powder, mp = 257–259°C (EtOH/DMF); IR (KBr) ν = 3413, 3259, 3207 (NH), 3009 (CH=), 2968 (CH-), 1591 (C=N) cm^{-1} ; ^1H NMR (DMSO- d_6) δ : 2.41 (s, 3H, CH₃), 7.08–8.26 (m, 9H, Ar-H), 10.54 (s, 1H, NH), 11.87 (s, 1H, NH), 12.49 (s, 1H, NH) ppm; ^{13}C -NMR (DMSO- d_6): δ : 18.7 (CH₃), 112.2, 113.4, 114.3, 115.7, 120.9, 121.1, 123.4, 123.9, 127.8, 128.1, 133.2, 134.2, 135.8, 137.4, 141.2, 160.4 (Ar-C) ppm; MS, m/z (%) 288 (M^+ , 32), 132 (20), 119 (25), 106 (100), 91 (70). Anal. Calcd. For C₁₇H₁₅N₅ (289.13): C, 70.57; H, 5.23; N, 24.20. Found: C, 70.33; H, 5.11; N, 24.11%.

3-[1-(2-(1H-Benzo[D]imidazol-2-Yl)hydrazono)ethyl]-2H-Chromen-2-One (3n)

Yellow powder, mp = 271–273°C (DMF); IR (KBr) ν = 3419 (NH), 2926 (CH-), 1721 (C=O), 1606 (C=N) cm^{-1} ; ^1H NMR (DMSO- d_6) δ : 2.47 (s, 3H, CH₃), 7.09–8.57 (m, 9H, Ar-H), 11.19 (s, 1H, NH), 12.48 (s, 1H, NH) ppm; ^{13}C -NMR (DMSO- d_6): δ : 18.7 (CH₃), 115.2, 115.9, 118.3, 121.9, 122.4, 123.3, 125.8, 126.1, 128.5, 131.2, 133.4, 135.2, 141.4, 149.2, 153.1, 158.4, 160.5 (Ar-C) ppm; MS, m/z (%) 318 (M^+ , 43), 144 (37), 126 (100), 78 (78), 64 (85). Anal. Calcd. For C₁₈H₁₄N₄O₂ (318.11): C, 67.92; H, 4.43; N, 17.60. Found: C, 67.83; H, 4.32; N, 17.41%.

3-[2-(1H-Benzo[D]imidazol-2-Yl)hydrazono]indolin-2-One (3o)³⁸

Yellow powder, mp = 305–307°C [lit. mp = 320°C] (DMF); IR (KBr) ν = 3419, 3201 (NH), 3076 (CH=), 2917 (CH-), 1680 (C=O), 1602 (C=N) cm^{-1} ; ^1H NMR (DMSO- d_6) δ : 7.03–7.81 (m, 8H, Ar-H), 9.51 (s, 1H, NH), 10.99 (s, 1H, NH), 12.48 (s, 1H, NH) ppm; ^{13}C -NMR (DMSO- d_6): δ : 115.5, 116.7, 123.9, 128.8, 128.9, 129.4, 129.5, 129.7, 130.0, 136.3, 140.8, 146.2, 151.4, 155.7 (Ar-C), 170.9 (C=O) ppm; MS, m/z (%) 277 (M^+ , 100), 198 (36), 182 (86), 153 (66), 75 (95). Anal. Calcd. For C₁₅H₁₁N₅O (277.10): C, 64.97; H, 4.00; N, 25.26. Found: C, 64.85; H, 3.91; N, 25.09%.

DFT Calculations

All computational calculations were performed using the Gaussian 09W software package.^{39,40} The molecular geometry of the studied compounds was optimized using the density functional theory B3LYP method, by implementing the standard 6–31G(d,p) basis set. The visualization of the optimized structures was performed using GaussView 6.0.1.^{41–44}

Frontier Molecular Orbitals and Global Reactivity Indexes

The Frontier Molecular Orbitals and the global descriptors of the investigated compounds were achieved under the same calculation level. Popular qualitative chemical concepts derived from conceptual DFT were measured to define the reactivity as well as the stability of a system^{45–51} (see Electronic [supplementary files](#)).

Antimicrobial Activity

The antimicrobial activity of the prepared compounds was tested using strains from the RCMB culture collection at Al-Azhar University, Egypt. The well-diffusion method assessed activity against Gram-positive bacteria (*Staphylococcus aureus*, *Bacillus subtilis*), Gram-negative bacteria (*Pseudomonas aeruginosa*, *Klebsiella pneumoniae*), and filamentous fungi (*Aspergillus gillus*, *Candida albicans*). Microbial cultures (10^8 cells/mL for bacteria, 10^5 cells/mL for fungi) were spread on agar plates, and 100 μ L of the compound solution (10 mg/mL) was added to 6 mm wells. Plates were incubated at 37°C for bacteria/yeast (24–48 h) and 28°C for fungi (48 h). Inhibition zones were measured, with larger zones indicating higher antimicrobial activity.⁵² DMSO served as a negative control, showing no inhibition, while ampicillin, gentamycin and nystatin were used as positive controls for bacteria and fungi, respectively.

Docking Methodology

The docking studies were carried out on Dell Inspiron 3847 [Intel(R) Core(TM) i7-4790 CPU @ 3.60GHz, 16GB of DIMM DDR3-1333/1600 memory, Windows 10 home (64 Bit)]. Molecular Operating Environment (MOE) package version 2022.02 (Chemical Computing Group, Inc. Molecular Operating Environment was used for performing docking studies).

Receptor Preparation

Docking procedures were performed using Crystal Structure of Mecr1 Extracellular Antibiotic-Sensor with open form-penicillin G (PDB: 2IWC), Phenylpyruvate Decarboxylase with Thiamine diphosphate (PDB: 2NXW), and CYP51 with Fluconazole (PDB: 1EA1) was obtained from protein data bank (PDB). The structures were first repaired, and then appropriately protonated in the presence of ligands using the Protonate 3D, energy minimized with force field: amber10: EHT until it reached an RMS (root mean square) gradient of 0.00001 kcal/mol/Å.

Ligand Preparation

Compounds **3c** and **3o** were built in ChemBioDraw Ultra 14.0 and sketched in MOE.

Docking Procedure

The MOE 2022.02 procedure's standard protocol was applied in this work. The Alpha Triangle placement determines the positions by randomly superposing ligand atom triplets alpha sphere dummies in the receptor site to create poses. The output database dock file, which was arranged according to the final score function (S), or the score of the final stage that was not set to zero, featured distinct poses for each ligand. The database browser was used to visually inspect the different poses of each ligand, and the best poses were chosen.

Conclusion

A green synthetic approach was applied to prepare a series of benzimidazole-based hydrazones using citric acid as an acid catalyst. These hydrazones **3a–o** were formulated as (E) configuration. The synthesized compounds, particularly **3c** and **3o**, exhibit promising antimicrobial activities against a range of pathogenic microorganisms. Their broad-spectrum efficacy, coupled with performance comparable to standard antimicrobial agents, underscores their potential as valuable additions to the arsenal against microbial infections. Molecular docking results suggest that specific structural features, such as electron-donating groups on aromatic rings (**3c**) and the presence of a heterocyclic moiety (**3o**), significantly influence antimicrobial efficacy. Increased lipophilicity also appears to enhance cell wall penetration and target binding. Future work may explore in vivo biological testing and structural optimization for enhanced selectivity and potency. Potential applications include the development of new antimicrobial agents with environmentally friendly synthetic

profiles. Limitations of this study include the absence of in vivo data and the need for broader antimicrobial screening to fully establish the therapeutic potential of these compounds.

Acknowledgments

The authors extend their appreciation to the Deanship of Scientific Research at Princess Nourah bint Abdulrahman University for the financial support and funding.

Funding

This work was funded by the Princess Nourah bint Abdulrahman University Researchers Supporting Project number (PNURSP2025R80), Princess Nourah bint Abdulrahman University, Riyadh, Saudi Arabia.

Disclosure

The authors declare no conflicts of interest in this work.

References

- Anastas PT, Warner JC. *Green Chemistry: Theory and Practice*. Oxford: Oxford University Press; 2000.
- Wagh YB, Tayade YA, Mahulikar PP, Dalal DS. Citric acid promoted green synthesis of bioactive heterocycles. *Curr Green Chem*. 2023;10(1):73–91. doi:10.2174/2213346110666230102120527
- Deshmukh MB, Patil SS, Jadhav SD, Pawar PB. Green approach for Knoevenagel condensation of aromatic aldehydes with active methylene group. *Synth Commun*. 2012;42(8):1177–1183. doi:10.1080/00397911.2010.537423
- Patil SS, Jadhav SD, Deshmukh MB. Eco-friendly and economic methods for Knoevenagel condensation by employing natural catalyst. *Indian J Chem Sect B*. 2013;52B:1172–1175.
- Yadav G, Mani JV. Green synthesis of Schiff bases by using natural acid catalysts. *Int J Sci Res*. 2015;4(2):121–127.
- Desai V, Shinde R. Green synthesis of nicotinic acid hydrazide Schiff bases and its biological evaluation. *Int J Pharm Sci Rev Res*. 2015;5(2):930–935.
- Dinore JM, Yelwande AA, Palve MP, Sapkal AV. Citric acid catalyzed synthesis of hydrazones Schiff bases of 2,4-dinitrophenyl hydrazine. *Int J Pharm Pharmaceut Res*. 2016;6(2):349–354.
- Nigam M, Tuttle D, Morra B, Dicks AP, Rodriguez J. Putting the squeeze on imine synthesis: citrus juice as a reaction medium in the introductory organic laboratory. *Green Chem Lett Rev*. 2023;16(1):2185107. doi:10.1080/17518253.2023.2185107
- Zhou JH, Chen X, Yang D, Liu CY, Zhou XZ. A facile and general oxidative hydroxylation of organoboron compounds: citric acid as an efficient catalyst in water to access phenolic and alcoholic motifs. *Molecules*. 2023;28(23):7915. doi:10.3390/molecules28237915
- Shaikh KA, Chaudhar UN, Ningdale VB. Citric acid catalyzed synthesis of amidoalkyl naphthols under solvent-free condition: an eco-friendly protocol. *J Appl Chem*. 2014;7(4):90–93. doi:10.9790/5736-07429093
- Shakoor A, Fareed G, Ahmad I, et al. Exploring the anti-diabetic activity of benzimidazole containing Schiff base derivatives: in vitro α -amylase, α -glucosidase inhibitions and in silico studies. *J Mol Struct*. 2025;1321:143136. doi:10.1016/j.molstruc.2024.140136
- Anichina K, Argirova M, Tzoneva R, et al. 1H-benzimidazole-2-yl hydrazones as tubulin-targeting agents: synthesis, structural characterization, anthelmintic and antiproliferative activity against MCF-7 cells. *Chem Biol Interact*. 2021;345:109540. doi:10.1016/j.cbi.2021.109540
- Işik A, Çevik UA, Çelik I, et al. Benzimidazole-hydrazone derivatives: synthesis, in vitro anticancer, antimicrobial, antioxidant activities, in silico DFT and ADMET studies. *J Mol Struct*. 2022;1270:133946. doi:10.1016/j.molstruc.2022.133946
- Kumar V, Basavarajaswamy G, Rai V, et al. Rapid 'one-pot' synthesis of a novel benzimidazole-5-carboxylate and its hydrazone derivatives as anti-inflammatory and antimicrobial agents. *Bioorg Med Chem Lett*. 2015;25(7):1420–1426. doi:10.1016/j.bmcl.2015.02.043
- Argirova M, Cherneva E, Mihaylov R, Momekov G, Yancheva D. New metal complexes of 1H-benzimidazole-2-yl hydrazones: cytostatic, proapoptotic and modulatory activity. *Arch Biochem Biophys*. 2025;764:110245. doi:10.1016/j.abb.2024.110245
- Mirgany TO, Motiur-Rahman AFM, Alanazi MM. Design, synthesis, and evaluation of benzimidazole-hydrazones as dual EGFR and HER2 inhibitors. *J Mol Struct*. 2024;1309:18177. doi:10.1016/j.molstruc.2024.138177
- Ulloora S, Shabaraya R, Ranganathan R, Adhikari VA. Synthesis, anticonvulsant and anti-inflammatory studies of new 1,4-dihydropyridin-4-yl-phenoxyacetohydrazones. *Eur J Med Chem*. 2013;70:341–349. doi:10.1016/j.ejmech.2013.10.010
- Melnyk P, Leroux V, Sergheraert C, Grellier P. Design, synthesis and in vitro antimalarial activity of an acylhydrazone library. *Bioorg Med Chem Lett*. 2006;16(1):31–35. doi:10.1016/j.bmcl.2005.09.058
- Garkani-Nejad Z, Ahmadi-Roudi B. Modeling the antileishmanial activity screening of 5-nitro-2-heterocyclic benzylidene hydrazides using chemometrics. *Eur J Med Chem*. 2010;45(2):719–726. doi:10.1016/j.ejmech.2009.11.019
- Küçüköglü K, Çevik UA, Nadaroglu H, et al. Synthesis and docking of N-acyl hydrazones-benzimidazole as hCA I and II inhibitors. *Med Chem*. 2023;19(5):485–494. doi:10.2174/1573406419666221222143530
- Waghmare PB, Shinde AB, Kshirsagar RP. Synthesis of pharmacologically potent benzimidazole analogs. *Polycycl Aromat Compd*. 2025;45:106–122. doi:10.1080/10406638.2024.2387615
- Khare A, Jain N, Singh RK. Synthetic approach to potential anticancer benzimidazole derivatives: a review. *Mini Rev Med Chem*. 2022;22(9):1289–1304. doi:10.2174/1389557521666211001122118
- Islam R, Koizumi F, Kodera Y, Inoue K, Okawara T, Masutani M. Design and synthesis of phenolic hydrazide hydrazones as potent PARG inhibitors. *Bioorg Med Chem Lett*. 2014;24(17):3802–3806. doi:10.1016/j.bmcl.2014.06.065

24. Thimmegoda NR, Nanjunda SS, Ananda KCS, Yip GW, Rangappa KS. Evaluation of benzimidazole derivatives as inhibitors of MDA-MB-231 cell proliferation. *Bioorg Med Chem Lett*. 2008;18(2):432–435. doi:10.1016/j.bmcl.2007.11.010
25. Gomha SM, Abolibda TZ, Alruwaili AH, et al. Efficient green synthesis of hydrazide derivatives using L-proline: characterization and docking studies. *Catalysts*. 2024;14(4):489. doi:10.3390/catal14040489
26. Gomha SM, Riyadh SM, Farag B, Al-Hussain SA, Zaki MEA, Mohamed MA. Green synthesis of hydrazone-thiazolones using vitamin B1 and their antibacterial implications. *Green Chem Lett Rev*. 2024;17(1):2380746. doi:10.1080/17518253.2024.2380746
27. Gomha SM, Riyadh SM, El-Sayed AAA, et al. Grinding-assisted synthesis of arylhydrazono curcumin analogues and bis-pyrazolines as CDK inhibitors. *Inorg Chem Commun*. 2024;169:113128. doi:10.1016/j.inoche.2024.113128
28. Gomha SM, Riyadh SM, Alharbi REK, Zaki MEA, Abolibda TZ, Farag B. Green synthesis and docking of azines using cellulose sulfuric acid under microwave irradiation. *Crystals*. 2023;13(2):260. doi:10.3390/cryst13020260
29. Alzahrani AYA, Gomha SM, Zaki MEA, Farag B, Abdelgawad FE, Mohamed MA. Chitosan–sulfonic acid catalyzed green synthesis of naphthalene-based azines as anticancer agents. *Future Med Chem*. 2024;16(8):647–663. doi:10.4155/fmc-2024-0034
30. Al-Humaidi JY, Gomha SM, Albedair LA, Zaki MEA, Mukhrish YE, Mohamed MA. Green synthesis and anticancer activity of bis-imidazole-thiazole hybrids targeting hepatocellular carcinoma. *Curr Org Synth*. 2025;22(3):371–382. doi:10.2174/1570179419666230822112027
31. Said MA, Riyadh SM, Al-Kaff NS, et al. Greener biological study of bis-thiadiazoles as potential COVID-19 drug candidates. *Arab J Chem*. 2022;15(9):104101. doi:10.1016/j.arabjc.2022.104101
32. Yaccoubi F, El-Naggar M, Abdelrazek FM, et al. Pyrido-pyrimido-thiadiazinones: green synthesis, docking, and biological evaluation as obesity inhibitors. *J Taibah Univ Sci*. 2022;16(1):1275–1286. doi:10.1080/16583655.2022.2093603
33. Al-Humaidi JY, Gomha SM, Abd El-Ghany NA, et al. Green synthesis and molecular docking study of some new thiazoles using terephthalohydrazide chitosan hydrogel as eco-friendly biopolymeric catalyst. *Catalysts*. 2023;13(10):1311. doi:10.3390/catal13101311
34. Abdallah AM, Gomha SM, Zaki MEA, Abolibda TZ, Kheder NAA. A green synthesis, DFT calculations, and molecular docking study of some new indeno[2,1-b]quinoxalines containing thiazole moiety. *J Mol Struct*. 2023;1292:136044. doi:10.1016/j.molstruc.2023.136044
35. Hussein AM, Gomha SM, El-Ghany NA A, et al. Green biocatalyst for ultrasound-assisted thiazole derivatives: synthesis, antibacterial evaluation, and docking analysis. *ACS Omega*. 2024;9(11):13666–13679. doi:10.1021/acsomega.4c00824
36. Akula G, Srinivas B, Vidyasagar M, Kandikonda S. Synthesis of 3-(1H-benzimidazol-2-yl amino)-2-phenyl-1,3-thiazolidin-4-one as potential CNS depressant. *Int J PharmTech Res*. 2011;3(1):360–364.
37. Bethi S, Vidyasagar M, Rajamanohar K, Rao V, Gummudavelly S. Synthesis and pharmacological evaluation of new benzimidazole derivatives. *Der Chem Sin*. 2011;2(1):84–90.
38. Badr MZA, Mahmoud AM, Mahgoub SA, Hozien ZA. Condensation and cyclization reactions of 2-hydrazinobenzimidazole, -benzoxazole, and -benzothiazole. *Bull Chem Soc Jpn*. 1988;61(4):1339–1344. doi:10.1246/bcsj.61.1339
39. Bhrigu B, Siddiqui N, Pathak D, Alam MS, Ali R, Azad B. Anticonvulsant evaluation of some newer benzimidazole derivatives: design and synthesis. *Acta Pol Pharm*. 2012;69(1):53–62.
40. Sharma K, Jain R. Synthesis of some novel 3-[(2-hydrazono)benzimidazolyl]-2-indolinones as possible azodyes. *Asian J Chem*. 1994;6(2):273–276.
41. Becke AD. A new mixing of Hartree–Fock and local density-functional theories. *J Chem Phys*. 1993;98(2):1372–1377. doi:10.1063/1.464304
42. Frisch MJ, Trucks GW, Schlegel HB, et al. *Gaussian 09, Revision A.02*. Wallingford CT: Gaussian, Inc; 2016.
43. Becke AD. Density-functional thermochemistry. III. The role of exact exchange. *J Chem Phys*. 1993;98(7):5648–5652. doi:10.1063/1.464913
44. Hehre WJ, Radom L, Schleyer PVR, Pople JA. *Ab Initio Molecular Orbital Theory*. New York: Wiley; 1986.
45. Lee C, Yang W, Parr RG. Development of the Colle–Salvetti correlation-energy formula into a functional of the electron density. *Phys Rev B*. 1988;37(2):785–789. doi:10.1103/PhysRevB.37.785
46. Ditchfield R, Hehre WJ, Pople JA. Self-consistent molecular-orbital methods. IX. An extended Gaussian-type basis for molecular-orbital studies of organic molecules. *J Chem Phys*. 1971;54(2):724–728. doi:10.1063/1.1674902
47. Parr RG, Yang W. *Density-Functional Theory of Atoms and Molecules*. New York: Oxford University Press; 1989.
48. Vela A, Gazquez JL. A relationship between the static dipole polarizability, the global softness, and the Fukui function. *J Am Chem Soc*. 1990;112(4):1490–1492. doi:10.1021/ja00160a044
49. Toro-Labbé A. Characterization of chemical reactions from the profiles of energy, chemical potential, and hardness. *J Phys Chem A*. 1999;103(23):4398–4403. doi:10.1021/jp984597v
50. Parr RG, Szentpály LV, Liu S. Electrophilicity index. *J Am Chem Soc*. 1999;121(9):1922–1924. doi:10.1021/ja983494x
51. Domingo LR, Chamorro E, Pérez P. Understanding the reactivity of captodative ethylenes in polar cycloaddition reactions: a theoretical study. *J Org Chem*. 2008;73(12):4615–4624. doi:10.1021/jo800572a
52. Al-Mutabagani LA, Abdelrazek FM, Gomha SM, et al. Synthesis and biological evaluation of thiazolyl-ethylidene hydrazino-thiazole derivatives: a novel heterocyclic system. *Appl Sci*. 2021;11(19):8908. doi:10.3390/app11198908

Drug Design, Development and Therapy

Publish your work in this journal

Drug Design, Development and Therapy is an international, peer-reviewed open-access journal that spans the spectrum of drug design and development through to clinical applications. Clinical outcomes, patient safety, and programs for the development and effective, safe, and sustained use of medicines are a feature of the journal, which has also been accepted for indexing on PubMed Central. The manuscript management system is completely online and includes a very quick and fair peer-review system, which is all easy to use. Visit <http://www.dovepress.com/testimonials.php> to read real quotes from published authors.

Submit your manuscript here: <https://www.dovepress.com/drug-design-development-and-therapy-journal>

Dovepress
Taylor & Francis Group